

Fitting the DESI BAO Data with Dark Energy Driven by the Cohen–Kaplan–Nelson Bound

Patrick Adolf^{1*}, Martin Hirsch^{2†}, Sara Krieg^{1‡}, Heinrich Päs^{1§}, Mustafa Tabet^{1¶}

¹*Fakultät für Physik, Technische Universität Dortmund, D-44221 Dortmund, Germany*

²*Instituto de Física Corpuscular (IFIC), Universidad de Valencia-CSIC, E-46980 Valencia, Spain*

June 17, 2024

Abstract

Gravity constrains the range of validity of quantum field theory. As has been pointed out by Cohen, Kaplan, and Nelson (CKN), such effects lead to interdependent ultraviolet (UV) and infrared (IR) cutoffs that may stabilize the dark energy of the universe against quantum corrections, if the IR cutoff is set by the Hubble horizon. As a consequence of the cosmic expansion, this argument implies a time-dependent dark energy density. In this paper we confront this idea with recent data from DESI BAO, Hubble and supernova measurements. We find that the CKN model provides a better fit to the data than the Λ CDM model and can compete with other models of time-dependent dark energy that have been studied so far.

1 Introduction

Quantum field theory (QFT) describes physics only in the absence of strong gravitational effects. A prominent example for the breakdown of QFT when this condition does not apply is that the maximum information stored in a space-time region scales with the volume in QFT while it scales holographically with the horizon area for black holes [1–6]. This consideration implies that QFT overcounts fundamental degrees of freedom for large energies and large length scales and has been employed by Cohen, Kaplan and Nelson (CKN) [7] to derive ultraviolet (UV) and infrared (IR) cutoffs that restrict the range of validity of QFT. Since the entropy of a black hole provides an upper bound for the entropy for any system, the entropy S_{QFT} within a box of size L described by QFT is constrained by the Bekenstein–Hawking entropy S_{BH}

$$S_{\text{QFT}} = \Lambda_{\text{UV}}^3 L^3 \leq \pi L^2 M_{\text{Pl}}^2 = S_{\text{BH}}, \quad (1)$$

where Λ_{UV} represents the UV cutoff, the maximum length L_{max} for a fixed Λ_{UV} defines the IR cutoff $\Lambda_{\text{IR}} = L_{\text{max}}^{-1}$ (and vice versa), and M_{Pl} denotes the Planck mass. However, as CKN have further pointed out, an effective field theory satisfying the Bekenstein bound of equation (1) still allows for the existence of numerous states with a Schwarzschild radius larger than the size of the box. This problem can be resolved by introducing a more stringent limit that excludes all states describing a black hole, the so-called “CKN bound” [7]

$$\Lambda_{\text{UV}}^4 \lesssim \frac{1}{L^2} M_{\text{Pl}}^2. \quad (2)$$

*patrick.adolf@tu-dortmund.de

†mahirsch@ific.uv.es

‡sara.krieg@tu-dortmund.de

§heinrich.paes@tu-dortmund.de

¶mustafa.tabet@tu-dortmund.de

While there exist several works that study the consequences of the CKN bound for particle phenomenology, such as the magnetic moment of leptons [8–12], the hierarchy problem [13] and the phenomenology of radiative neutrino masses [14], one of the first applications of the CKN bound that has already been discussed in the original CKN paper [7] is the cosmological constant problem [15]. After the recent result of the Dark Energy Spectroscopic Instrument (DESI) [16] in combination with other cosmological data has provided new hints that the dark energy density of the universe may be time-dependent, we focus here on the consequences of the CKN bound for the evolution of dark energy. According to QFT, quantum corrections to the dark energy density scale with $\sim \Lambda_{\text{UV}}^4$, where Λ_{UV} is the UV cutoff of the corresponding theory. If the Planck scale is chosen as the UV cutoff of the Standard Model, this leads to a correction that is many orders of magnitudes larger than the observed dark energy density. One possibility to resolve this problem is to assume that QFT ceases to work at a cutoff scale $\Lambda_{\text{UV}} \ll M_{\text{Pl}}$. Accordingly, CKN have suggested to adopt the Hubble horizon, i.e. the inverse Hubble parameter as the IR cutoff of QFT, $L_{\text{max}} = 1/H$, resulting in a UV cutoff $\Lambda_{\text{UV}} \sim 10^{-3} \text{ eV}$ that corresponds to the observed dark energy density $\rho_{\Lambda} \sim (10^{-3} \text{ eV})^4$ observed today. While this scenario may stabilize the dark energy of the universe against large quantum corrections, it also entails the prediction that these quantum corrections to the dark energy density are time dependent, as the Hubble parameter is not a constant.

In the following, we review evolving dark energy due to the CKN bound, address arguments in the literature that the model may not produce the correct equation of state for an accelerated universe, and perform a global analysis that fits the model to the recent DESI BAO and supernova datasets. For other recent works that discuss evolving dark energy explanations of the DESI data, see for example [17–21].

This paper is organized as follows: In section 2, we solve the Friedmann equations for the CKN case, and provide a brief overview of alternative dark energy models against which we compare the CKN model. In section 3, we introduce the statistical approach adopted and present the results of a global analysis that confronts evolving dark energy models with DESI BAO, Hubble and supernova data and compares them to the standard Λ CDM paradigm that describes cosmology with a dominating constant dark energy density or cosmological constant Λ and a subdominant component of cold dark matter (CDM). We also discuss the expected improvements from new data anticipated for the next few years. Finally, we summarize and discuss our findings in section 4.

2 Evolving Dark Energy Models and the CKN Bound

The recent analysis of measurements of the DESI baryonic acoustic oscillations (BAO) data, combined with data from the cosmological microwave background (CMB) and Pantheon+, Union3, or DES-SN5YR datasets probing supernova distances results in a 3.9σ evidence for time-varying dark energy models compared to the Λ CDM paradigm [16]. In the following, we analyze the evolution of the dark energy density in the presence of a UV and IR cutoff satisfying the CKN bound in equation (2), and compare the behavior with alternative evolving dark energy models.

Adopting an IR cutoff of the Hubble horizon size, it follows from equation (2) that

$$\Lambda_{\text{UV}}^4 \lesssim H^2(z) M_{\text{Pl}}^2, \quad (3)$$

with the redshift z , Planck mass M_{Pl} , and the Hubble constant $H(z)$. This in turn yields for the vacuum energy density (VED) $\rho_{\text{VED}}^{1\text{-loop}}$ at 1-loop

$$\rho_{\text{VED}}^{1\text{-loop}}(z) \simeq \nu \frac{\Lambda_{\text{UV}}^4}{16\pi^2} = \nu \frac{M_{\text{Pl}}^2 H^2(z)}{16\pi^2}. \quad (4)$$

Here, an additional parameter ν has been introduced, such that the VED of the original CKN bound is recovered for $\nu = 1$. In the following, we refer to $\nu = 1$ as the CKN case; otherwise, we refer to the ν CKN case.

This generalization serves two purposes. First, in the derivation of equation (3), several prefactors have been dropped such as a $1/2$ coming from the Schwarzschild radius. Further, the derivation of equation (4) depends on the particle content of the underlying theory, such as possible dark matter candidates. Moreover, the more general equation (4) applies also for other dark energy models discussed in the literature where the vacuum energy scales proportional to $H^2(z)$ such as running vacua models [22–24] or holographic dark energy models [25–27], see reference [28] for a review.

To arrive at equation (4), we have neglected the IR cutoff $\Lambda_{\text{IR}}^4 \propto H(z)^4$. Given that we are only analyzing data where $H(z)^4 \ll M_{\text{Pl}}^2 H(z)^2$, this simplification is justified. Note, that we neglect the neutrino masses and that heavy particles with masses above the UV cutoff do not contribute [7, 8].

While it has been argued in the literature that a scaling proportional to $H^2(z)$ according to equation (4) leads to a wrong equation of state that does not explain the accelerated expansion of the universe [25, 29], this conclusion holds only as far as the conservation of energy is assumed to hold separately for the individual matter and dark energy contributions. Dropping this assumption yields a modified equation of state (see e.g. [30–32]) that leads to accelerated expansion and does in fact, as we will show, provide an excellent fit to data in the range of redshifts up to $z \sim \mathcal{O}(1)$.

Moreover, it has been pointed out in reference [29] that a $H^2(z)$ scaling may conflict with processes at large z such as CMB data or large structure formation. However, this behavior may be alleviated by a matter component starting to become dominant around $z \sim 0.4$ and a small prefactor $\nu \lesssim 1$ in the ν CKN model. In fact, as the prefactor depends in general on the concrete particle physics model, it is unknown how the parameter ν evolves with time or redshift.

To study the consequences of the CKN bound for the evolution of the universe, we introduce the correction term from equation (4) semi-classically into the energy–momentum tensor $T^{\mu\nu}$ [15]:

$$T_{\text{tot}}^{\mu\nu} = T_{\text{classical}}^{\mu\nu} + \langle T^{\mu\nu} \rangle, \quad (5)$$

with

$$\langle T^{\mu\nu} \rangle = \rho_{\text{VED}}^{1\text{-loop}} g^{\mu\nu}. \quad (6)$$

Here, $T_{\text{classical}}^{\mu\nu}$ contains the contributions from matter, radiation and the classical cosmological constant. It is important to note that matter and dark energy are no longer conserved separately but can transform into each other. Such effects of matter non-conservation have been discussed for example in references [30, 32]. Otherwise, the Bianchi identity $\nabla_{\mu} G^{\mu\nu} = 0$, where G denotes the Einstein tensor, together with the conservation of the classical energy–momentum tensor, would imply that:

$$\nabla_{\mu} \langle T^{\mu\nu} \rangle = 0 \Rightarrow \dot{\rho}_{\text{VED}}^{1\text{-loop}} = 0, \quad (7)$$

which is in contradiction with the time dependence of the VED, cf. reference [33] for further discussion.

This leads to the Friedmann equation

$$H^2(t) = \frac{8\pi G}{3} (\rho_{\text{M}}(t) + \rho_{\Lambda}(t)), \quad (8)$$

with the matter density $\rho_{\text{M}}(t)$ and the dark energy density $\rho_{\Lambda}(t) = \rho_{\text{VED}}(t) + \Lambda_0$, where Λ_0 is a constant term in the Einstein field equations, and Newton’s constant G . Moreover, we neglect radiation as we are only interested in the matter-dominated era, and consider a spatially flat universe, i.e. $\Omega_{\text{k}} = 0$. The conservation of the energy–momentum tensor yields

$$\dot{\rho}_{\Lambda}(t) + \dot{\rho}_{\text{M}}(t) = -3H(t)\rho_{\text{M}}(t). \quad (9)$$

Solving equations (8) and (9) we obtain

$$H^2(z) = H_0^2 (\Omega_{\text{M}}(z) + \Omega_{\Lambda}(z)), \quad (10)$$

where $H_0 \equiv H(z=0)$ denotes today’s value of the Hubble constant and

$$\Omega_{\text{M}}(z) = \Omega_{\text{M}}^0 (1+z)^{3-\frac{\nu}{2\pi}}, \quad (11)$$

$$\Omega_{\Lambda}(z) = \Omega_{\Lambda}^0 + \Omega_{\text{M}}^0 \frac{\nu}{6\pi - \nu} \left[(1+z)^{3-\frac{\nu}{2\pi}} - 1 \right], \quad (12)$$

where Ω_{M}^0 and Ω_{Λ}^0 denote the matter and dark energy density today normalized to $\rho_{\text{crit},0} = 8\pi G/(3H_0^2)$, respectively. For $\nu > 0$ one finds the dark energy behavior typical for many quintessence models [34].

In the following, we briefly discuss several alternative dark energy models that we are going to compare with the CKN and ν CKN cases in section 3. The Friedmann equation for a spatially flat universe in the matter dominated epoch for the most common models can usually be written as follows [35]:

$$\frac{H^2(z)}{H_0^2} = \Omega_M^0 (1+z)^3 + f_{\text{DE}}(z), \quad (13)$$

where the matter density parameter Ω_M^0 indicates the proportion of matter relative to the critical density of the universe today, $\rho_{\text{crit},0}$, and $f_{\text{DE}}(z)$ describes the dark energy evolution in the universe. One can define a relationship between the density ρ and pressure p , expressed through a parameter ω as $p = \omega\rho$. When ω is a constant, this equation is referred to as equation of state. In the general case ω can be written as:

$$\omega(z) = -1 + \frac{1}{3} \frac{d \ln f_{\text{DE}}(z)}{d \ln (1+z)}, \quad (14)$$

where $\omega < -1/3$ leads to an accelerated expansion of the universe corresponding to dark energy. Several cosmological models result from different values and parametrizations of ω . In particular, we are interested in the following three models that we compare against the CKN cases in the subsequent section.

Λ CDM Model In the standard cosmological model, a cosmological constant Λ is introduced into the Einstein field equations, which in turn leads to a constant dark energy. This corresponds to the choice of $\omega = -1$, i.e. $p = -\rho$, which yields

$$f_{\text{DE}}^{\Lambda\text{CDM}}(z) = \Omega_{\text{DE},0}^{\Lambda\text{CDM}}, \quad (15)$$

where $\Omega_{\text{DE},0}^{\Lambda\text{CDM}}$ denotes the present-day dark energy density in the Λ CDM model.

ω CDM Model In addition to matter and radiation, there may be for example other potential sources contributing to the energy-momentum tensor, which can only be explained by $\omega \neq -1$ like e.g. scalar fields in inflation models [36]. This results in a dark energy that is no longer constant in time. Therefore, ω becomes a free parameter of the model and one can derive

$$f_{\text{DE}}^{\omega\text{CDM}}(z) = \Omega_{\text{DE},0}^{\omega\text{CDM}} (1+z)^{3(1+\omega)}, \quad (16)$$

where $\Omega_{\text{DE},0}^{\omega\text{CDM}}$ is the present-day dark energy density in the ω CDM model. If experiments show that $\omega \neq -1$, this would indicate a time-varying dark energy.

$\omega_0\omega_a$ CDM Model To incorporate the dynamics of dark energy into a model, the parametrization $\omega(a) = \omega_0 + \omega_a(1-a)$ has been derived [37], where $a = (1+z)^{-1}$ is the scale factor. This leads to

$$f_{\text{DE}}^{\omega_0\omega_a\text{CDM}}(z) = \Omega_{\text{DE},0}^{\omega_0\omega_a\text{CDM}} (1+z)^{3(1+\omega_0+\omega_a)} e^{-3\omega_a(1-1/(1+z))}, \quad (17)$$

with the present-day dark energy density $\Omega_{\text{DE},0}^{\omega_0\omega_a\text{CDM}}$ in the $\omega_0\omega_a$ CDM model. It is evident that for $\omega_a = 0$ one recovers the ω CDM model.

In the following, we assume for all models $\Omega_M^0 + \Omega_{\text{DE},0} = 1$.

3 Comparison with Experimental Data

In this section, we perform a global analysis to determine the agreement of the CKN bound with current experimental data in particular in light of the recent DESI measurements [16]. Firstly, in section 3.1 we list and briefly discuss the datasets we use while in section 3.2 the statistical approach is explained. Finally, our results are presented in section 3.3.

3.1 Experimental Input

In our numerical analysis, the dataset from DESI BAO [16] is used in combination with model-independent Hubble measurements [38]. Additionally, two supernova distance datasets are used: Pantheon+ [39], and the DES-SN5YR [40] dataset which we denote as DESY5 in the following.

DESI BAO Baryonic acoustic oscillations are fluctuations in the density of baryonic matter, caused by acoustic density waves in the primordial plasma of the early universe. The corresponding observables are extracted from CMB data and can be found in reference [16]. There, they provide measurements and correlations for the comoving distance over the drag epoch D_M/r_d and the distance variable D_H/r_d . Here, r_d denotes the drag epoch, which is the distance sound can travel in the time from the Big Bang till the decoupling of the baryons. In cases with low signal-to-noise ratio instead the angle-average quantity D_V/r_d is provided. Note, that with DESI BAO data alone only the combination $r_d H_0$ can be constrained. Here, we keep the drag epoch r_d a free parameter in the fit. The dataset consists of seven bins with negligible correlations, cf. reference [16], between the overlapping bins.

Supernova Type Ia supernovae are considered as standard candles for determining cosmological distances. When distances are measured, Hubble’s parameter can be inferred using the formula for the physical distance. Here, we consider the datasets from Pantheon+ and DESY5. Unfortunately, the Union3 data is not publicly available.

For DESY5 the distance modulus and corresponding covariance matrices are taken from reference [40]. Note, that the unknown absolute magnitude M always appears with the Hubble constant H_0 such that the supernovae dataset alone cannot be used to determine H_0 . Thus, analogous to reference [40], we redefine the absolute magnitude M and Hubble parameter H_0 into one single parameter $\tilde{M} = M + 5 \log_{10}(c/H_0)$ over which we marginalize analytically. Here, c denotes the speed of light.

The Pantheon+ data and corresponding covariance matrices are taken from reference [39]. Here, again, we analytically marginalize over \tilde{M} and analogous to reference [16], we consider supernovae with redshifts $z > 0.01$.

Model-Independent Hubble Parameter Measurements An additional method, independent of specific cosmological models, exists for measuring the Hubble parameter. This involves utilizing gamma-ray bursts, introducing a correlation between their spectral characteristics and energy levels. Consequently, gamma-ray bursts serve as model-independent distance indicators, capable of spanning a significantly broader range of redshifts compared to supernovae. The data for these measurements is taken from reference [38]. Unfortunately, only the covariance matrix of Moresco et al. is provided [41] which, however, also contains the biggest source of correlation.

Note, that for this initial analysis, we neglect CMB data from temperature, polarization, and lensing measurements. In our approach, we fit all three experiments simultaneously, incorporating one supernova dataset at a time. By including the model-independent Hubble measurements, we also lift the afore-mentioned degeneracies in the parameters.

3.2 Statistical Procedure

To quantify the agreement between the different models, in particular the CKN cases and the experimental datasets listed in section 3.1, we perform a χ^2 test. In order to determine the best-fit point, we minimize the function

$$\chi^2 = \left(\vec{\mathcal{O}}_{\text{th}}(\xi_i) - \vec{\mathcal{O}}_{\text{exp}} \right)^T C^{-1} \left(\vec{\mathcal{O}}_{\text{th}}(\xi_i) - \vec{\mathcal{O}}_{\text{exp}} \right), \quad (18)$$

where the vector $\vec{\mathcal{O}}_{\text{th}}$ denotes the theory predictions as a function of the model parameters ξ_i , while the corresponding measurements with the covariance matrix C are denoted by the vector $\vec{\mathcal{O}}_{\text{exp}}$. Note, that equation (18) in its compact form does not yet account for the analytical marginalization we perform for the DESY5 and Pantheon+ likelihood, also see references [40, 42]. Despite the Bayesian nature of the underlying datasets, a

Table 1: Results of the best-fit points for the CKN and ν CKN case to the datasets of DESI BAO and Hubble, once combined with DESY5 and once with Pantheon+ data. Shown are the results for Hubble-today H_0 , the matter density parameter Ω_M^0 , the drag epoch r_d , the parameter ν and the minimal χ_{\min}^2 over the degrees of freedom (DOF).

Model/Datasets	H_0 /(km/s/Mpc)	Ω_M^0	r_d /Mpc	ν	χ_{\min}^2 /DOF
CKN					
+ DESY5	68.69 ± 2.39	0.354 ± 0.012	144.54 ± 4.89	–	1677/1871
+ Pantheon+	69.24 ± 2.41	0.344 ± 0.012	144.38 ± 4.89	–	1440/1632
νCKN					
+ DESY5	68.66 ± 2.38	0.354 ± 0.021	144.60 ± 4.87	1.00 ± 0.46	1677/1870
+ Pantheon+	67.94 ± 2.51	0.329 ± 0.021	147.76 ± 5.28	0.60 ± 0.49	1440/1631

Table 2: Contribution of the different experiments to the total χ_{\min}^2 from table 1 for the combination with DESY5 and Pantheon+.

Models	DESY5			Pantheon+		
	$\chi_{\min}^{2,\text{BAO}}$	$\chi_{\min}^{2,\text{DESY5}}$	$\chi_{\min}^{2,\text{Hubble}}$	$\chi_{\min}^{2,\text{BAO}}$	$\chi_{\min}^{2,\text{Pantheon+}}$	$\chi_{\min}^{2,\text{Hubble}}$
CKN	14.48	1649	12.86	14.37	1413	12.67
ν CKN	14.48	1649	12.85	13.51	1413	13.08

χ^2 statistics is a reasonable approximation as the provided uncertainties are Gaussian and the theoretical models are linear to a good approximation. Thus, we estimate the uncertainties and covariance matrix using the Hessian matrix at the minimum of the χ^2 distribution. We also provide the frequentist confidence levels (CL) by calculating the corresponding χ^2 contours which are determined for a given parameter plane of interest, by minimizing the χ^2 function for every grid point with respect to the remaining parameters.

We also compare CKN with other cosmological models, namely Λ CDM, ω CDM and $\omega_0\omega_a$ CDM introduced in section 2, by calculating the difference $\Delta\chi^2 = \chi_{\min}^{2,(\nu)\text{CKN}} - \chi_{\min}^{2,\text{alt.model}}$. For this comparison and assuming that Wilk’s theorem holds, $\Delta\chi^2$ follows a χ^2 distribution corresponding to the difference in the number of model parameters, respectively. This allows us to convert the $\Delta\chi^2$ values into the corresponding significances in terms of the one dimensional normal distribution. Note, however, that Wilk’s theorem only holds for comparisons between nested models, otherwise the provided significances only serve as an estimate. In particular, the $\Delta\chi^2$ values between the ν CKN case and the ω CDM model, as well as the CKN case and Λ CDM model cannot be converted into a significance this way. However, for the latter case the significance values between the ν CKN case and the Λ CDM model provide an estimate. In order to also quantify the agreement between the non-nested models, we compare the models using the differences in the Akaike information criterion (AIC) that quantifies the quality of the models fitting the data and also penalizes an increasing number of model parameters [43] with

$$\text{AIC} = \chi_{\min}^2 + 2k, \quad (19)$$

where k is the number of model parameters.

3.3 Results

In table 1 we show the best-fit points of the CKN model to the DESI BAO+Hubble datasets, each combined with either DESY5 or Pantheon+. The individual contribution of each experiment is given in table 2. It is already evident from the χ_{\min}^2 /DOF values that the CKN as well as the ν CKN model are well compatible

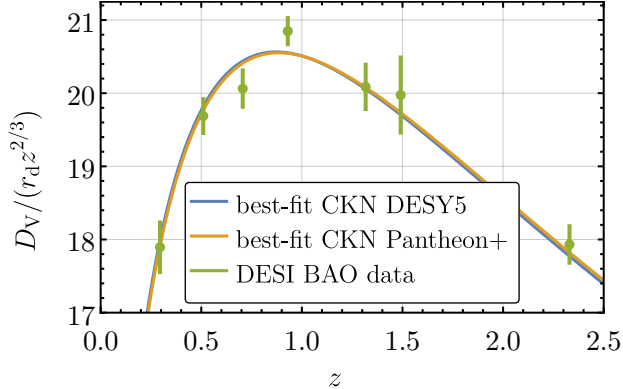


Figure 1: Shown is the angle-averaged distance quantity $D_V/(r_d z^{2/3})$ at our best-fit point together with the corresponding DESI measurements [16]. Since the results of the CKN and ν CKN model are too similar to see any difference, we only show the CKN model.

Table 3: Comparison between CKN and ν CKN and the alternative cosmological models. Shown is the difference $\Delta\chi^2 = \chi_{\min}^{2,(\nu)\text{CKN}} - \chi_{\min}^{2,\text{alt.model}}$ for both datasets, the significance as well as the difference ΔAIC . The negative values denote a preference of CKN and ν CKN over the alternative models, respectively. See text for the missing entries.

Models	$\Delta\chi_{\text{DESY5}}^2$	Significance	ΔAIC	$\Delta\chi_{\text{Pantheon+}}^2$	Significance	ΔAIC
CKN with						
Λ CDM	-4.6	-	-4.6	-1.1	-	-1.1
ω CDM	2.3	1.5σ	0.3	1.5	1.2σ	-0.2
$\omega_0\omega_a$ CDM	5.3	1.8σ	1.3	2.1	1.0σ	-1.9
νCKN with						
Λ CDM	-4.6	-2.1σ	-2.5	-1.2	-1.1σ	0.8
ω CDM	2.3	-	2.3	1.4	-	1.4
$\omega_0\omega_a$ CDM	5.3	2.3σ	3.4	2.0	1.4σ	0.0

with the data. This is substantiated by the best-fit which for the CKN as well as the ν CKN case is given by $\chi_{\min}^2/\text{DOF} \approx 0.90$ for the DESY5 dataset and $\chi_{\min}^2/\text{DOF} \approx 0.88$ for the Pantheon+ dataset. Additionally, we show the angle-averaged distance quantity $D_V/(r_d z^{2/3})$ at our best-fit point together with the corresponding DESI measurements in figure 1.

The quantitative comparison of the CKN and the ν CKN model with the Λ CDM, ω CDM and $\omega_0\omega_a$ CDM model is presented in table 3. There, we provide the difference $\Delta\chi^2$ of the best-fit points, the corresponding significance value and the difference in AIC. The other models are fitted using the same approach as for the CKN and ν CKN case. The resulting best-fit points are presented in table 4 and the procedure was compared with similar analyses in the literature where we find excellent agreement. Due to the fact that Wilk's theorem is not always applicable some entries in table 3 are missing. Therefore, for the comparison of non-nested models one should be careful interpreting the provided significances. Nevertheless, they still provide an estimation. Already from the $\Delta\chi^2$ value, it is clear that both the CKN and the ν CKN case provide a better explanation of the data compared to the Λ CDM model, for both datasets. However, for the Pantheon+ dataset the difference turns out to be non-significant. For the DESY5 dataset, both the $\Delta\chi^2$ and AIC indicate that the ω CDM and $\omega_0\omega_a$ CDM model perform slightly better than our models. However, for the Pantheon+ dataset, the CKN model actually turns out to describe the data slightly better than all other models according to the AIC with

Table 4: Results of the best-fit points from the Λ CDM, ω CDM and $\omega_0\omega_a$ CDM model to the datasets of DESI BAO and Hubble, once with DESY5 and once with Pantheon+ data. Shown are the results for Hubble-today H_0 , the matter density parameter Ω_M^0 , the drag epoch r_d , the parameters ω_0 and ω_a , and the minimal χ_{\min}^2 over the degrees of freedom (DOF).

Model /Datasets	H_0 in km/s/Mpc	Ω_M^0	r_d in Mpc	ω or ω_0	ω_a	χ_{\min}^2/DOF
ΛCDM						
+ DESY5	69.15 ± 2.41	0.320 ± 0.011	144.55 ± 4.90	–	–	1681/1871
+ Pantheon+	69.79 ± 2.44	0.308 ± 0.011	144.41 ± 4.89	–	–	1441/1632
ωCDM						
+ DESY5	68.71 ± 2.39	0.296 ± 0.014	144.27 ± 4.89	-0.874 ± 0.046	–	1674/1870
+ Pantheon+	69.43 ± 2.43	0.296 ± 0.014	144.26 ± 4.88	-0.921 ± 0.048	–	1438/1631
$\omega_0\omega_a$CDM						
+ DESY5	66.93 ± 2.40	0.334 ± 0.016	147.57 ± 5.17	-0.716 ± 0.093	-1.36 ± 0.65	1671/1869
+ Pantheon+	69.65 ± 2.43	0.312 ± 0.018	143.79 ± 4.86	-0.873 ± 0.076	-0.51 ± 0.58	1438/1630

the largest difference between the CKN case and the $\omega_0\omega_a$ CDM model.

We also compare the evolution of the dark energy density of the alternative models at the best-fit points with the 1σ band in figure 2 with the CKN case and in figure 3 with the ν CKN case. It can be observed that the qualitative evolution of the dark energy density is similar across all models, and the corresponding dark energy densities largely overlap within their 1σ bands.

Finally, the correlation at 95% and 68% CL for both dataset combinations for $\Omega_M^0-H_0$, H_0-r_d , $\Omega_M^0-r_d$ are provided in figure 4 for the CKN. Moreover, the correlations for $\nu-\Omega_M^0$, $\nu-H_0$, $\nu-r_d$ are shown in figure 5 for the ν CKN case.

Future Projection

In the near future, DESI will continue collecting data for another three years, and other experiments such as Euclid [44, 45], which started measuring last year, and the Large Synoptic Survey Telescope (LSST) at the Vera Rubin Observatory will begin gathering data [46]. This will result in significantly better statistics, smaller uncertainties, and thus allow for a more significant discrimination between the various cosmological models. Euclid is expecting an improvement on the uncertainties of cosmological model parameters by up to a factor of 10 [45].

We thus perform a rough estimation of the χ^2 difference between the different models that can be anticipated with future data. We assume that the central values of the experimental data stays the same, but with reduced uncertainties. In the case of the DESI BAO measurements, we reduce the uncertainties of the year-1 data release by $\sqrt{5}$ in order to account for the planned 5 years duration. In the case of the running Euclid experiment, we only consider the distance luminosity measurements. In order to account for the expected statistics, we rescale the uncertainties of the DESY5 and Pantheon+ datasets with a global factor. This factor is extracted from the projected reduction of the uncertainties on the model parameters of the ω CDM model [45]. In order to be conservative, we take the lowest improvement, which leads to a reduction by a factor 4. In table 5 we show the χ^2 differences between the (ν)CKN and the alternative models for the DESI projection, called DESI-5Y, the Euclid projection, and the combined projections for both, the DESY5 and Pantheon+ datasets. In table 6 we also show the corresponding significances. While DESI-5Y does not show a significant difference between the models, the combination of DESI-5Y and the Euclid projection looks promising in distinguishing between Λ CDM and all time-varying dark energy models considered in this work.

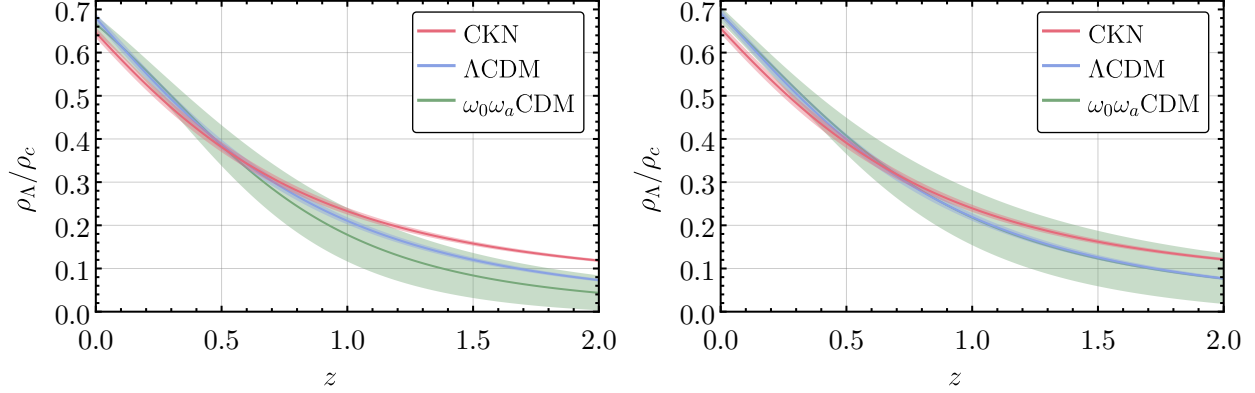


Figure 2: Shown is the evolution of the dark energy density ρ_Λ with the 1σ band in the CKN case in comparison with the Λ CDM, and $\omega_0\omega_a$ CDM model for the datasets DESI BAO+Hubble+DESY5 (left) and DESI BAO+Hubble+Pantheon+ (right) normalized to the critical density $\rho_c(z)$.

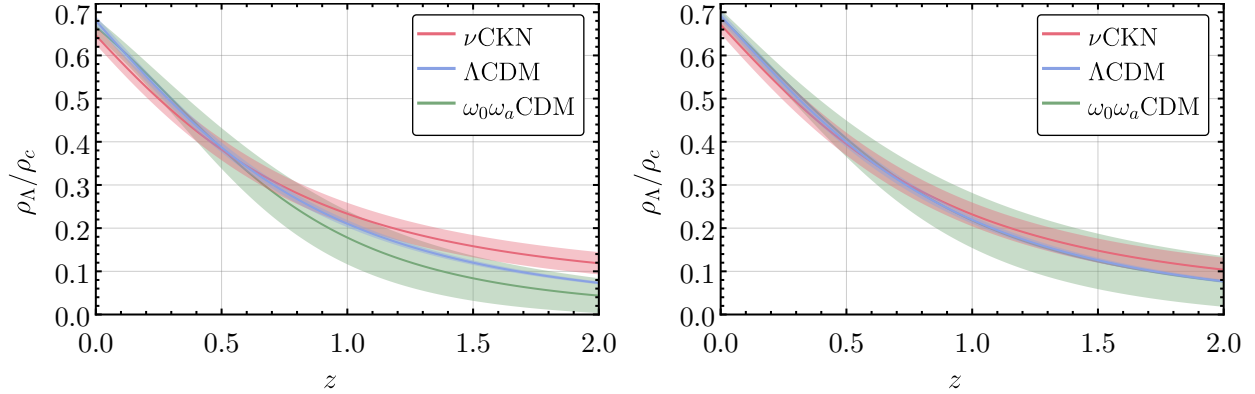


Figure 3: As figure 2, for the ν CKN case.

Table 5: Shown is the future projection of the results of the DESI experiment after five years of measurements (DESI-5Y) and the Euclid experiment. We compare the χ^2_{\min} difference between the CKN and ν CKN model to the other models studied in this work for both datasets: DESY5 and Pantheon+.

Models	DESI-5Y		Euclid		DESI-5Y + Euclid	
	$\Delta\chi^2_{\text{DESY5}}$	$\Delta\chi^2_{\text{Pantheon+}}$	$\Delta\chi^2_{\text{DESY5}}$	$\Delta\chi^2_{\text{Pantheon+}}$	$\Delta\chi^2_{\text{DESY5}}$	$\Delta\chi^2_{\text{Pantheon+}}$
CKN with						
Λ CDM	-1.8	3.9	-16.5	-9.4	-42.4	-17.4
ω CDM	7.1	7.4	14.9	1.5	20.4	7.1
$\omega_0\omega_a$ CDM	18.4	11.1	47.0	1.5	45.4	8.1
νCKN with						
Λ CDM	-3.7	-1.0	-18.1	-9.4	-43.2	-19.0
ω CDM	5.1	2.5	13.3	1.5	19.6	5.5
$\omega_0\omega_a$ CDM	16.4	6.2	45.4	1.5	44.6	6.5

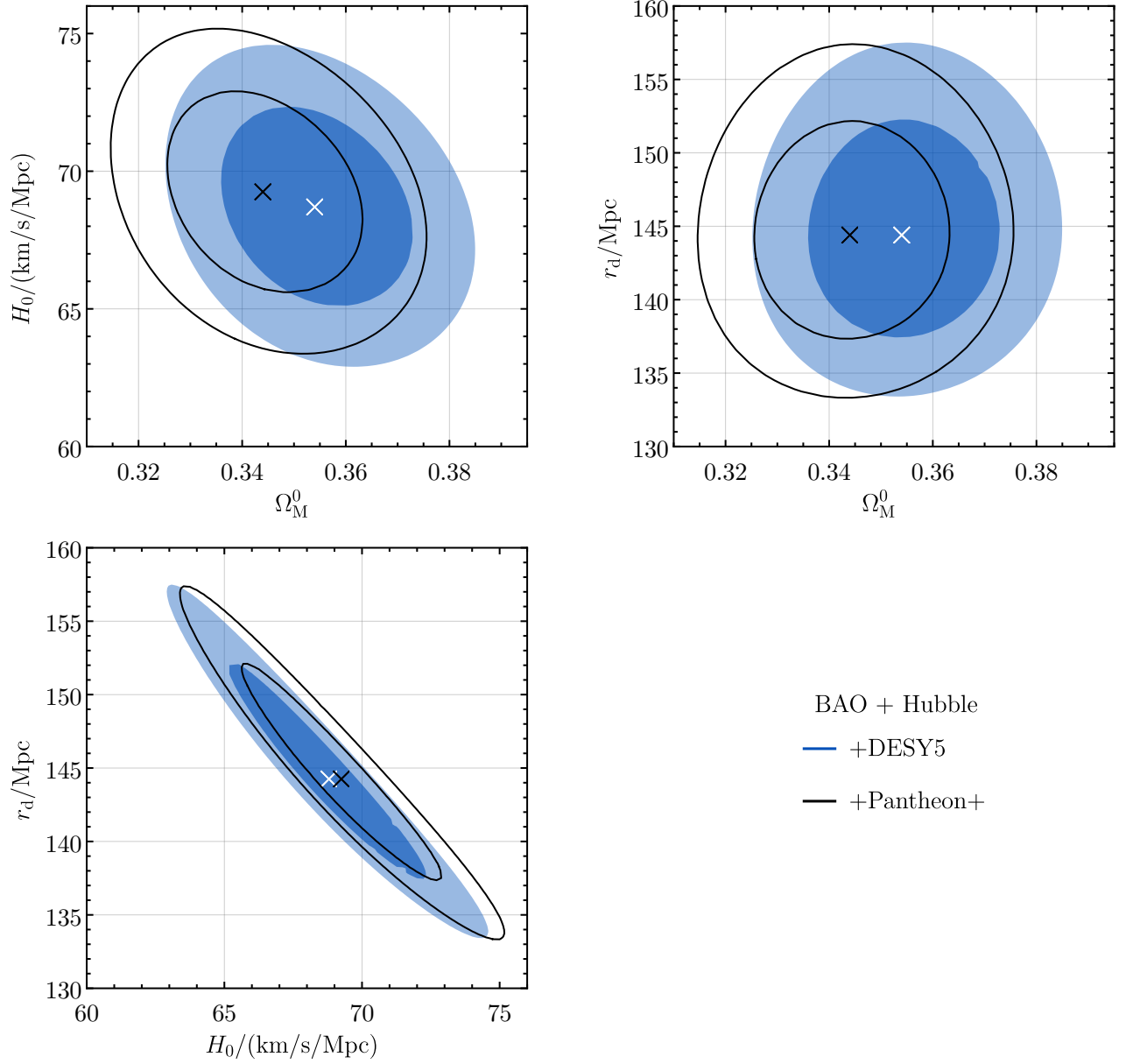


Figure 4: Correlations of H_0 - Ω_M^0 (top left), H_0 - r_d (top right), r_d - Ω_M^0 (bottom left) in the CKN model for the DESI BAO+Hubble+DESY5 (blue area) and DESI BAO+Hubble+Pantheon+ (black lines) dataset at the 95% and 68% CL.

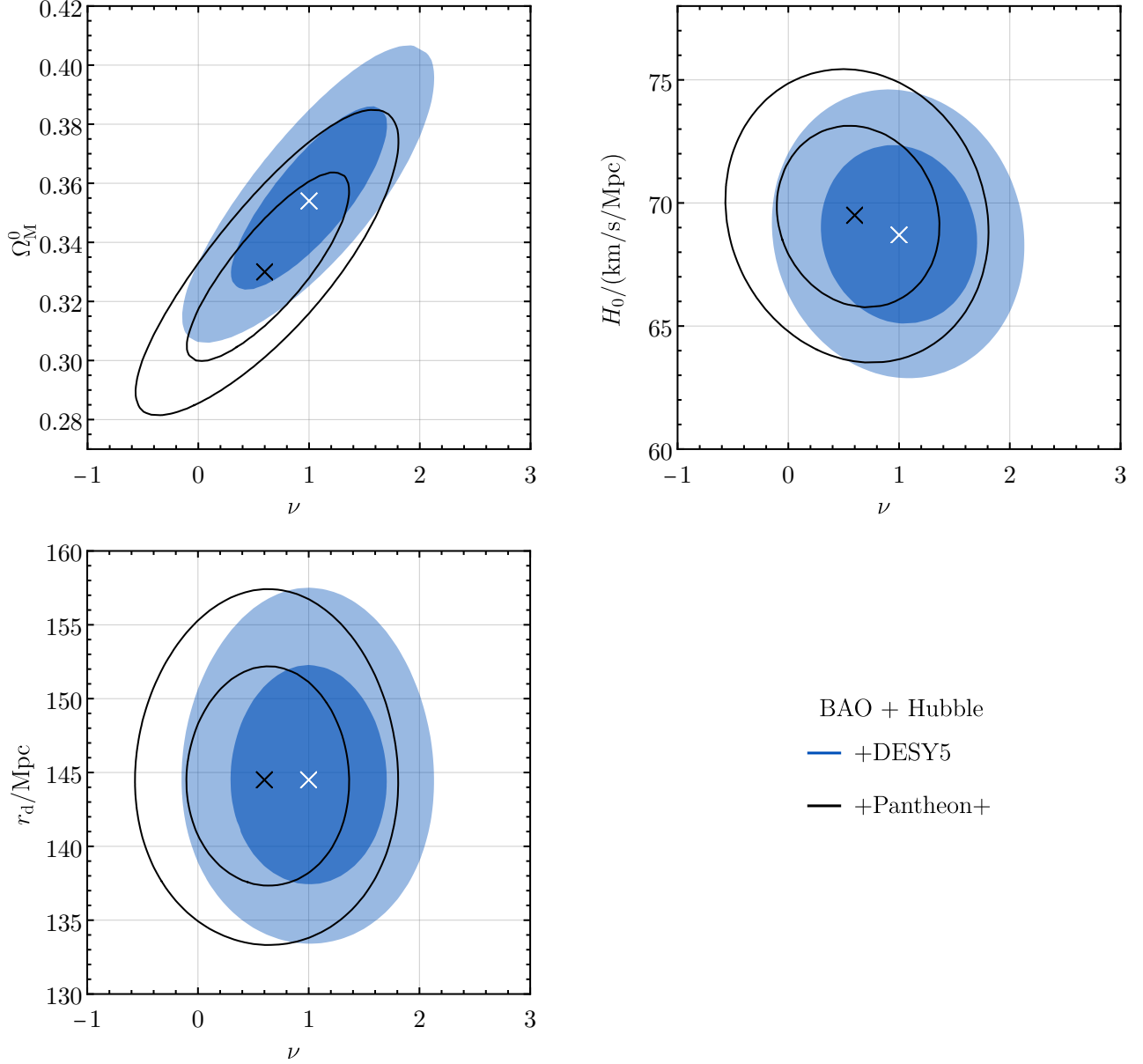


Figure 5: Correlations of ν - Ω_M^0 (top left), ν - H_0 (top right), ν - r_d (bottom left) in the ν CKN model for the DESI BAO+Hubble+DES5 (blue area) and DESI BAO+Hubble+Pantheon+ (black lines) datasets at the 95% and 68% CL.

Table 6: Shown is the future projection of the results of the DESI experiment after five years of measurements (DESI-5Y) and the Euclid experiment. We convert the χ^2_{\min} difference in table 5 into significances Σ , see text for details.

Models	DESI-5Y		Euclid		DESI-5Y + Euclid	
	Σ_{DESY5}	$\Sigma_{\text{Pantheon+}}$	Σ_{DESY5}	$\Sigma_{\text{Pantheon+}}$	Σ_{DESY5}	$\Sigma_{\text{Pantheon+}}$
CKN with						
ΛCDM	–	–	–	–	–	–
ωCDM	2.7σ	2.7σ	3.9σ	1.2σ	4.5σ	2.7σ
$\omega_0\omega_a\text{CDM}$	3.9σ	2.9σ	6.5σ	0.7σ	6.4σ	2.4σ
$\nu\text{CKN with}$						
ΛCDM	-1.9σ	-1.0σ	-4.3σ	-3.1σ	-6.6σ	-4.4σ
ωCDM	–	–	–	–	–	–
$\omega_0\omega_a\text{CDM}$	4.0σ	2.5σ	6.7σ	1.2σ	6.7σ	2.5σ

4 Summary and Discussion

In this study, we have explored the cosmological consequences of the CKN bound and performed a global analysis of cosmological data from the DESI BAO analysis combined with DES-SN5YR (DESY5) or Pantheon+ supernova data. In order to account for unknown prefactors and to include alternative models where the dark energy density scales with H^2 , we have generalized the CKN model to the νCKN model. Due to the overlaps between the DESY5 and Pantheon+ datasets, we have considered only one supernova dataset at a time. Remarkably, the CKN model is found to provide a good fit to the data, even preferred over the ΛCDM model. Despite the additional model parameter, the νCKN model did not provide a better fit compared to the CKN model. For the DESI BAO data combined with the Pantheon+ dataset, the CKN model provides a better fit than all alternative models considered in this work. These results demonstrate the need for a more comprehensive analysis, possibly incorporating power spectra and lensing information from CMB measurements and assessing compatibility with the early universe through big bang nucleosynthesis data. Moreover, new data expected to be released in the next few years will improve the statistics dramatically. A projection of the change of the presently allowed parameter regions with the projected improved statistics justifies the expectation that it will be possible to discriminate the (ν)CKN model from the ΛCDM model with a statistical significance up to 6.6σ and from $\omega_0\omega_a\text{CDM}$ up to 6.7σ .

In summary, the CKN bound that addresses the restriction gravity poses on the validity of QFT has intriguing cosmological consequences. These consequences are now starting to be probed by new cosmological data.

Acknowledgements

P.A. was supported by the *Cusanuswerk* during the early stages of this work, and later on by the *Studienstiftung des deutschen Volkes*. M.H. acknowledges support by grants PID2020-113775GB-I00 (AEI/10.13039/501100011033) and CIPROM/2021/054 (Generalitat Valenciana).

References

- [1] J. D. Bekenstein, *Black holes and entropy*, *Phys. Rev. D* **7** (1973) 2333–2346.
- [2] J. D. Bekenstein, *Generalized second law of thermodynamics in black hole physics*, *Phys. Rev. D* **9** (1974) 3292–3300.
- [3] J. D. Bekenstein, *A Universal Upper Bound on the Entropy to Energy Ratio for Bounded Systems*, *Phys. Rev. D* **23** (1981) 287.
- [4] J. D. Bekenstein, *Entropy bounds and black hole remnants*, *Phys. Rev. D* **49** (1994) 1912–1921, [gr-qc/9307035].
- [5] S. W. Hawking, *Particle Creation by Black Holes*, *Commun. Math. Phys.* **43** (1975) 199–220.
- [6] S. W. Hawking, *Black Holes and Thermodynamics*, *Phys. Rev. D* **13** (1976) 191–197.
- [7] A. G. Cohen, D. B. Kaplan and A. E. Nelson, *Effective field theory, black holes, and the cosmological constant*, *Phys. Rev. Lett.* **82** (1999) 4971–4974, [hep-th/9803132].
- [8] A. G. Cohen and D. B. Kaplan, *Gravitational contributions to the electron g -factor*, 2103.04509.
- [9] T. Banks and P. Draper, *Remarks on the Cohen-Kaplan-Nelson bound*, *Phys. Rev. D* **101** (2020) 126010, [1911.05778].
- [10] J. Bramante and E. Gould, *Anomalous anomalies from virtual black holes*, *Phys. Rev. D* **101** (2020) 055007, [1911.04456].
- [11] N. Blinov and P. Draper, *Densities of states and the Cohen-Kaplan-Nelson bound*, *Phys. Rev. D* **104** (2021) 076024, [2107.03530].
- [12] J. Bramante and E. Gould, *Material matter effects in gravitational UV/IR mixing*, *Phys. Rev. D* **101** (2020) 084022, [1910.07905].
- [13] T. W. Kephart and H. Päs, *UV/IR Mixing, Causal Diamonds and the Electroweak Hierarchy Problem*, 2209.03305.
- [14] P. Adolf, M. Hirsch and H. Päs, *Radiative neutrino masses and the Cohen-Kaplan-Nelson bound*, *JHEP* **11** (2023) 078, [2306.15313].
- [15] S. Weinberg, *The Cosmological Constant Problem*, *Rev. Mod. Phys.* **61** (1989) 1–23.
- [16] DESI collaboration, A. G. Adame et al., *DESI 2024 VI: Cosmological Constraints from the Measurements of Baryon Acoustic Oscillations*, 2404.03002.
- [17] A. NOTARI, M. REDI AND A. TESI, *Consistent Theories for the DESI dark energy fit*, 2406.08459.
- [18] I. D. GIALAMAS, G. HÜTSI, K. KANNIKE, A. RACIOPPI, M. RAIDAL, M. VASAR AND H. VEERMÄE, *Interpreting DESI 2024 BAO: late-time dynamical dark energy or a local effect?*, 2406.07533.
- [19] R. CAMILLERI et al. [DES], *The Dark Energy Survey Supernova Program: Investigating Beyond- Λ CDM*, 2406.05048.
- [20] M. VAN RAAMSDONK AND C. WADDELL, *Holographic motivations and observational evidence for decreasing dark energy*, 2406.02688.
- [21] N. ROY, *Dynamical dark energy in the light of DESI 2024 data*, 2406.00634.
- [22] M. Rezaei, M. Malekjani and J. Sola, *Can dark energy be expressed as a power series of the Hubble parameter?*, *Phys. Rev. D* **100** (2019) no.2, 023539, [1905.00100].

- [23] M. Rezaei, J. Solà Peracaula and M. Malekjani, *Cosmographic approach to Running Vacuum dark energy models: new constraints using BAOs and Hubble diagrams at higher redshifts*, *Mon. Not. Roy. Astron. Soc.* **509** (2021) 2593–2608, [2108.06255].
- [24] I. L. Shapiro and J. Sola, *Scaling behavior of the cosmological constant: Interface between quantum field theory and cosmology*, *JHEP* **02** (2002) 006, [hep-th/0012227].
- [25] M. Li, *A Model of holographic dark energy*, *Phys. Lett. B* **603** (2004) 1, [hep-th/0403127].
- [26] E. Telali and E. Saridakis, *Power-law holographic dark energy and cosmology*, *The European Physical Journal C* **82** (05, 2022) .
- [27] U. K. Tyagi, S. Haridasu and S. Basak, *Holographic and Gravity-Thermodynamic Approaches in Entropic Cosmology: Bayesian Assessment using late-time Data*, 2406.07446.
- [28] E. Abdalla et al., *Cosmology intertwined: A review of the particle physics, astrophysics, and cosmology associated with the cosmological tensions and anomalies*, *JHEAp* **34** (2022) 49–211, [2203.06142].
- [29] S. D. H. Hsu, *Entropy bounds and dark energy*, *Phys. Lett. B* **594** (2004) 13–16, [hep-th/0403052].
- [30] J. Sola, *Cosmological constant and vacuum energy: old and new ideas*, *J. Phys. Conf. Ser.* **453** (2013) 012015, [1306.1527].
- [31] C. Moreno-Pulido and J. Sola Peracaula, *Equation of state of the running vacuum*, *Eur. Phys. J. C* **82** (2022) 1137, [2207.07111].
- [32] D. Pavon and W. Zimdahl, *Holographic dark energy and cosmic coincidence*, *Phys. Lett. B* **628** (2005) 206–210, [gr-qc/0505020].
- [33] J. Sola Peracaula, *The cosmological constant problem and running vacuum in the expanding universe*, *Phil. Trans. Roy. Soc. Lond. A* **380** (2022) 20210182, [2203.13757].
- [34] I. Zlatev, L.-M. Wang and P. J. Steinhardt, *Quintessence, cosmic coincidence, and the cosmological constant*, *Phys. Rev. Lett.* **82** (1999) 896–899, [astro-ph/9807002].
- [35] DESI collaboration, K. Lodha et al., *DESI 2024: Constraints on Physics-Focused Aspects of Dark Energy using DESI DR1 BAO Data*, 2405.13588.
- [36] J. D. Barrow and S. Cotsakis, *Inflation Without a Trace of Lambda*, *Eur. Phys. J. C* **80** (2020) 839, [1907.02928].
- [37] E. V. Linder, *Exploring the expansion history of the universe*, *Phys. Rev. Lett.* **90** (2003) 091301, [astro-ph/0208512].
- [38] A. Favale, M. G. Dainotti, A. Gómez-Valent and M. Migliaccio, *Towards a new model-independent calibration of Gamma-Ray Bursts*, 2402.13115.
- [39] D. Brout et al., *The Pantheon+ Analysis: Cosmological Constraints*, *Astrophys. J.* **938** (2022) 110, [2202.04077].
- [40] DES collaboration, T. M. C. Abbott et al., *The Dark Energy Survey: Cosmology Results With ~1500 New High-redshift Type Ia Supernovae Using The Full 5-year Dataset*, 2401.02929.
- [41] M. Moresco, R. Jimenez, L. Verde, A. Cimatti and L. Pozzetti, *Setting the Stage for Cosmic Chronometers. II. Impact of Stellar Population Synthesis Models Systematics and Full Covariance Matrix*, *Astrophys. J.* **898** (2020) 82, [2003.07362].
- [42] M. Goliath, R. Amanullah, P. Astier, A. Goobar and R. Pain, *Supernovae and the nature of the dark energy*, *Astron. Astrophys.* **380** (2001) 6–18, [astro-ph/0104009].

- [43] H. Akaike, *A new look at the statistical model identification*, *IEEE Transactions on Automatic Control* **19** (1974) 716–723.
- [44] EUCLID collaboration, R. Laureijs et al., *Euclid Definition Study Report*, 1110.3193.
- [45] Y. MELLIER *et al.* [EUCLID], *Euclid. I. Overview of the Euclid mission*, 2405.13491.
- [46] LSST collaboration, v. Ivezić et al., *LSST: from Science Drivers to Reference Design and Anticipated Data Products*, *Astrophys. J.* **873** (2019) 111, [0805.2366].